Supplementary Material:

Mechanism of actin filament pointed end capping by tropomodulin

Jampani Nageswara Rao, Yadaiah Madasu, Roberto Dominguez*

Department of Physiology, Perelman School of Medicine, University of Pennsylvania, Philadelphia, Pennsylvania 19104, USA

This PDF file includes:

Materials and Methods

Proteins. Actin (*30*) and TM (*31*) were purified from rabbit skeletal muscle**.** The cDNA encoding for human Tmod1 (UniProt: P28289) was synthesized (GENEWIZ). Full length gelsolin was purchased (Cytoskeleton, Inc.). The cDNA encoding for human gelsolin (UniProt: P06396) and human CP α and β isoforms (UniProt: P52907 and P47756-2) were purchased (ATCC). Human Tmod1 fragments 50-101 (ABS1) and 160-349 (ABS2) were fused, via a 9-aa linker (GGSGGSGGS), C-terminally to human gelsolin segment 1 (GS1, residues 52-176) by overlap PCR. The fusion constructs, as well as the individual ABS1 and ABS2 domains, were cloned between the SapI and EcoRI sites of vector pTYB11 (New England BioLabs). Full-length Tmod1 was cloned between the NdeI and SapI sites of vector pTYB1 (New England BioLabs). CP α and β isoforms were cloned respectively into multiple cloning sites 2 and 1 of vector pRSFDuet-1 (Novagen), which includes a multi-histidine affinity purification tag and a TEV cleavage site in cloning site 1. Point mutations were introduced using the QuickChange mutagenesis kit (Qiagen).

All the proteins were expressed in BL21(DE3) cells (Invitrogen), grown in Terrific Broth medium at 37°C until the OD_{600} reached a value of 1.5-2.0. Expression was induced with addition of 1 mM isopropylthio-β-D-galactoside, and was carried out for 16 h at 18°C. Cells were harvested by centrifugation, re-suspended in 20 mM Tris-HCl (pH 8.0), 300 mM NaCl, 0.5 mM EDTA, 1 mM PMSF and lysed using a microfluidizer apparatus (Microfluidics). All the proteins (except CP$\alpha\beta$) were first purified on a chitin affinity column, and eluted after self-cleavage of the intein induced by incubation with 50 mM DTT for 16 h. Proteins were additionally purified through a SD200HL 26/600 gel filtration column (GE Healthcare) in 20 mM HEPES, pH 7.5, 50 mM NaCl, and 1 mM DTT. The CP$\alpha\beta$ heterodimer was purified on a Ni-NTA affinity column. The affinity tag was then removed by cleavage with TEV protease and additional purification through an ion exchange MonoQ column (Pharmacia) in 20 mM HEPES (pH 7.5), 1 mM DTT and a 50-300 mM NaCl gradient.

Crystallization, data collection and structure determination. Actin crystallography is complicated by the natural tendency of actin to polymerize under most crystallization conditions. Monomeric actin structures have been obtained with several proteins and small molecules that form stable, soluble complexes with actin, including DNAse I (*32*), profilin (*33*), gelsolin (*34*), vitamin D-binding protein(*35*), toxofilin (*36*), twinfilin (*37*), latrunculin-A (*38*) and other marine macrolides (*39*). An alternative solution, chemical crosslinking of actin

with tetramethylrhodamine (*40*), was used to obtain the structure of monomeric actin (*40*), as well as that of its complex with the FH2 domain of the yeast formin Bni1p (*41*). Mutagenesis of actin has also been used to prevent polymerization during crystallization of actin alone (*42*) as well as its complex with *Vibrio*'s VCD (*26*). Co-crystallization of actin complexes with two actin-binding proteins that interact with different surfaces on the actin monomer has been used to obtain the structures of the WH2 domain (*35*) and that of the ternary complex of actin, profilin and the GAB domain of VASP (*43*). Finally, the realization that gelsolin and the WH2/Tβ4 domain share a homologous region, the LKKT motif, allowed for the crystallization of a GS1-Tβ4 fusion protein in complex with actin that revealed the structure of the C-terminal portion of Tβ4 (*44*).

Here, we also used GS1 fusions with the two actin-binding sites of Tmod, after establishing that the proteins could simultaneously bind monomeric actin when not fused (Fig. 1 B and C and fig. S2). Fusion was only used here as a way to increase the affinity of the individual Tmod domains for monomeric actin. But, because gelsolin and Tmod do not share any homologous region, we used a 9-aa flexible linker between GS1 and the two Tmod fragments. The Tmod fragments extended beyond the actin-binding sites defined in previous biochemical studies (*9, 16-18*). Thus, ABS1 and ABS2 comprised human Tmod1 residues 50-101 and 160-349, respectively (Fig. 1A). The last 10 residues of Tmod1 were not included, because they are not present in other isoforms, a choice later justified by the structure. The linker (GGSGGSGGS) was chosen such that it could span the distance between the barbed and pointed ends of the actin monomer. Because GS1 binds at the barbed end of the actin monomer, which is mostly inaccessible in the filament, it was not expected to interfere with Tmod interactions at the pointed end of the TM-coated filament.

Actin at 60 μM in 2 mM Tris-HCl (pH 7.5), 0.2 mM $CaCl_2$, 0.2 mM ATP, 1 mM NaN_3 (G-buffer) and the GS1-Tmod fusion constructs in 20 mM HEPES (pH 7.5), 50 mM NaCl, 1 mM DTT were mixed at 1:1.2 molar ratio. The complexes were dialyzed into 20 mM HEPES (pH 7.5), 50 mM NaCl, 0.2 mM $CaCl_2$, 0.2 mM ATP, 1 mM DTT, and concentrated to ~8 mg mL^{-1}. Samples were centrifuged at 278,000 × *g* for 30 min before crystallization to remove potential aggregates. Crystals of the complexes were obtained at 16°C using the hanging drop vapor diffusion method and 4 μL drops (2 μL protein solution and 2 μL well solution). For ABS1 the well solution contained 0.18 M NaF, 11% (w/v) PEG 3350, 1% (v/v) PEG 1000, and 1% (v/v) PEG 400. Crystals of ABS1 in complex with ADP-actin were obtained under

identical conditions, by first dialyzing actin into G-buffer in which ATP was replaced by 4 mM ADP, and with addition of 4 mM $CaCl_2$, 20 unit mL^{-1} hexokinase, and 1 mM glucose. For ABS2, the well solution consisted of 0.25 M NaCl, 12% (w/v) PEG 3350, and 0.2 μL Silver Bullet HT condition E10 (Hampton Research). X-ray datasets were collected at 100 K at beamline X6A of the National Synchrotron Light Source (Brookhaven National Laboratory, Upton, New York, USA). The diffraction datasets were indexed and scaled with the program HKL2000 (HKL Research). Molecular replacement solutions were obtained with the program Phenix (*45*) using PDB entries 1EQY and 1IO0 as search models. Model building and refinement were carried out with the programs Coot (*46*) and Phenix (*45*).

The structure of GS1-ABS1 bound to ADP-actin was refined at 2.15 Å resolution. While the crystallization conditions were the same as for ATP-actin, the crystals were different, and contained four complexes in the asymmetric unit (table S1). Two of the complexes were poorly defined, and did not display density for ABS1. The remaining two complexes were well defined, but one showed only residues 58-74 of ABS1, and only one complex showed ABS1 in full, displaying a conformation very similar to that observed with ATP-actin. Crystals of ABS2 could not be obtained with ADP-actin.

Isothermal titration calorimetry. ITC measurements were carried out on a VP-ITC apparatus (MicroCal). Samples were dialyzed for 2 days against 20 mM HEPES (pH 7.5), 50 mM NaCl, 0.2 mM $CaCl_2$, 0.2 mM ATP, 1 mM DTT. Titrations were done at two different temperatures (10 and 20°C) and with ATP- or ADP-bound actin:GS1. Titrations consisted of 10 μL injections, lasting for 10 s and spaced 300 s apart. The concentration of the titrant was 10- to 20-fold higher than that of the binding partner in the 1.44 mL cell. The heat of binding was corrected for the small exothermic heat of injection, determined by injecting ligand into buffer. Data were analyzed with the program Origin (OriginLab Corporation) using a one-site binding model.

Barbed- and pointed-end elongation and depolymerization assays. To measure the pointed end capping activity of wild type and mutant Tmod variants, the barbed end must be tightly capped, because faster dynamics at this end can mask subunit exchange at the pointed end. Traditionally, gelsolin has been used to cap the barbed end in Tmod studies (*7, 10, 12, 16-18, 47-49*). However, in sarcomeres and erythrocytes Tmod works in conjunction with other barbed end capping proteins, namely CP and adducin (*3, 4*). To establish optimal,

physiologically relevant conditions for our experiments, we first compared the barbed end capping activities of gelsolin and CP in elongation and depolymerization assays.

Filament barbed end elongation was monitored using the pyrene-actin polymerization assay (*50*) on a Cary Eclipse fluorescence spectrophotometer (Varian). Actin filament seeds were prepared by polymerizing 10 μM actin in 10 mM Tris (pH 7.5), 1 mM $MgCl_2$, 50 mM KCl, 1 mM EGTA, 0.1 mM NaN_3, 0.02 mg mL^{-1} BSA, 0.2 mM ATP (F-buffer) for 2 h at 23°C, followed by the addition of 20 μM phalloidin and centrifugation at 435,000 x *g* for 20 min. The pellet fraction was re-suspended in 3 × F-buffer to a final concentration of 6 μM, and passed five times through a 27½-gauge syringe needle to shear the actin filaments. The re-suspended F-actin seeds were then allowed to re-anneal overnight. The elongation experiments were carried out in F-buffer, and in the presence of 1.5 μM phalloidin-stabilized filament seeds, 0.5 μM actin monomers (6% pyrene-labeled), and increasing concentrations of CP or gelsolin. Note that the concentration of actin monomers was below the critical concentration for monomer addition at the pointed end (0.6 μM), but above that of the barbed end (0.1 μM), such that monomer addition could only occur at the barbed end. Data acquisition started 10 s after mixing. All the measurements were done at 25°C. Control experiments were carried out with addition of buffer alone. In these experiments, as little as 25 nM CP was sufficient to block filament growth, whereas filaments still grew in the presence of 250 nM gelsolin (fig. S6, A and B).

Depolymerization was measured using the pyrene-actin assay (*50*) as the fluoresce decrease resulting from monomer dissociation from 0.5 μM actin filaments. The actin filaments were prepared by polymerization of 2 μM monomeric actin (12% pyrene-labeled) in F-buffer for 2 h at 23°C. We monitored the depolymerization of filaments pre-incubated for 10 min at 23°C with increasing concentrations of CP or gelsolin (fig. S6, C and D). Filaments depolymerized only slightly faster in the presence of CP, which stops barbed end addition but not pointed end dissociation. In contrast, depolymerization increased with increasing gelsolin concentration, which can be attributed to the other activities of gelsolin – severing and monomer sequestration. Combined, the results of the elongation and depolymerization assays suggested that CP and not gelsolin should be used in Tmod capping experiments.

Therefore, in subsequent pointed end elongation assays, the barbed ends of 1.5 μM phalloidin-stabilized filament seeds were capped with 25 nM CP two minutes before

polymerization. The experiments were carried out in F-buffer, and in the presence of 1.5 μM actin monomers (6% pyrene-labeled). To establish the optimal concentration of TM for these experiments, we monitored elongation in the presence of 50 nM Tmod and increasing TM concentrations. Pointed end elongation decreased with TM concentration, reaching equilibrium at 1 μM TM (fig. S6E). This effect depended exclusively on TM's interaction with Tmod, since TM had no effect on pointed end elongation in the absence of Tmod or barbed end capping by CP (fig. S6F). TM did marginally improve barbed end capping by gelsolin in elongation (fig. S6G) and depolymerization (fig. S6H) assays, likely through inhibition of filament severing (*51*).

Because of the faster kinetics of elongation, we used this assay rather than depolymerization for analysis of the Tmod mutants. The general conditions for elongation assays were established based on the results of the experiments above: 1.5 μM G-actin (6% pyrene-labeled), 1.5 μM phalloidin-stabilized filament seeds, 25 nM CP and 1 μM TM. Polymerization rates were calculated as the slope of the polymerization curve between 0.1 and 0.4 of the maximum fluorescence normalized to the actin control, and converted to nM s^{-1} (nM monomers adding to filaments s^{-1}), assuming a total concentration of polymerizable actin of 0.9 μM (*50*) using the equation Rate (nM s^{-1}) = 0.9 X slope X 1000. The K_D values for Tmod binding to the pointed end (± TM) were obtained using a one site-binding model with the program GraphPad Prism (GraphPad Software Inc.).

Modeling of Tmod at the pointed end. The structures of ABS1 and ABS2 were superimposed, respectively, onto the first and second protomers at the pointed end of the actin filament model (*21*), which was the only arrangement that did not produce steric hindrance between the two Tmod domains (fig S3 and main text). This arrangement additionally placed the N-termini of ABS1 and ABS2 near the N-termini of the two TM coiled coils on each side of the filament, such that the two TM-binding sites of Tmod were ideally positioned for interactions with TM (fig S5). Finally, this model was supported by extensive mutagenesis (Fig. 2).

Importantly, to produce this model we used the 6.6 Å resolution EM structure of the filament (*21*), which is very similar to that obtained at comparable resolution from x-ray fiber diffraction (*52*), but different from that of the pointed end resulting from single particle EM analysis (*53*). According to the latter structure, the major difference observed at the pointed

end is a tilting motion of ~12° of the first subunit towards the second subunit, whereas the rest of the subunits display the classical filamentous structure. This tilting motion produces minor clashes between the first subunit of the filament and Tmod's ABS2 when it is bound to the second subunit. Moreover, the resolution of the EM structure of the pointed end is only 23 Å, which is in part the result of intrinsic limitations of single particle analysis when applied to the relatively small particle that constitutes the pointed end. Finally, although this structure focuses specifically on the pointed end, it lacks two key elements that define the pointed end within the context of Tmod's function, TM and Tmod. In particular, the proposed tilting of the first subunit will impact TM's interactions that occur semi-repeatedly along seven subunits of the long-pitch helix of the filament (*23*). For all these reasons, we did not use this structure to model Tmod at the pointed end, and used instead the higher resolution structures of the filament (*21, 52*).

Compared to monomeric actin, actin subunits in the filament are characterized by a flatter conformation, resulting from a ~12° propeller rotation of the outer domain (comprised of subdomains 1 and 2) with respect to the inner domain (subdomains 3 and 4) (*21, 52*). However, this rotation may not occur at the pointed end, where the actin subunits are exposed, and thus unconstrained. Therefore, we did not attempt to alter the conformation of actin observed in the structures of the complexes with GS1-ABS1 and GS1-ABS2, which is that of the actin monomer, after superimposition at the pointed end.

The two TM-binding sites of Tmod have been previously defined through mutagenesis and biochemical analysis (*10, 48*). Secondary structure analysis of Tmod's N-terminal region (residues 1-160) was performed using the program Quick2D (http://toolkit.tuebingen.mpg.de/quick2_d) that combines the results of several secondary structure prediction algorithms. The various algorithms all predicted a similar secondary structure composition for the two TM-binding sites, consisting of three helical segments (Fig. 3A). They also accurately predicted the helical segment of ABS1, observed in the crystal structure. The predicted helical segments of the two TM-binding sites were modeled as ideal α-helices using the sequence of human Tmod1, and were connected by flexible linkers according to the secondary structure prediction using the program Coot (*46*). The models of the two TM-binding sites were then connected N-terminally to ABS1 and ABS2, and positioned such that they contacted the two TM coiled coils on each side of the filaments. The position of TM used in the model is that of the 'blocked' state, which corresponds to the minimum energy position of TM when bound to the filament in the absence of myosin and troponin, or with Ca^{+2}-free troponin (*22, 23, 54*). We anticipate that the loops connecting the

TM- and actin-binding sites of Tmod are flexible enough to allow for the azimuthal sliding of TM on the filament upon Ca^{+2} binding to troponin and myosin-binding to the filament. The resulting model of the pointed end was then subjected to energy regularization with the program Phenix (*45*), by fixing the conformation of actin and TM, and allowing only the Tmod atoms to move during energy minimization (the final model is displayed in Fig. 3)

Calculation of protein-protein contact areas. The interface areas of Tmod interactions with the first three subunits of the actin filament were calculated with the program PISA (*55*), using the online server http://www.ebi.ac.uk/pdbe/prot_int/pistart.html. The interface area is calculated as the difference in the total accessible surface areas of the interacting proteins in isolation and in the complex divided by two. Note that while the interface areas for the complexes of ABS1 and ABS2 with the first and second protomers of the filament, respectively, are precisely determined from the structures, the contacts of ABS2 with protomers 1 and 3 are only approximately estimated based on the superimposition of the structure onto the filament model (*21*).

Fig. S1

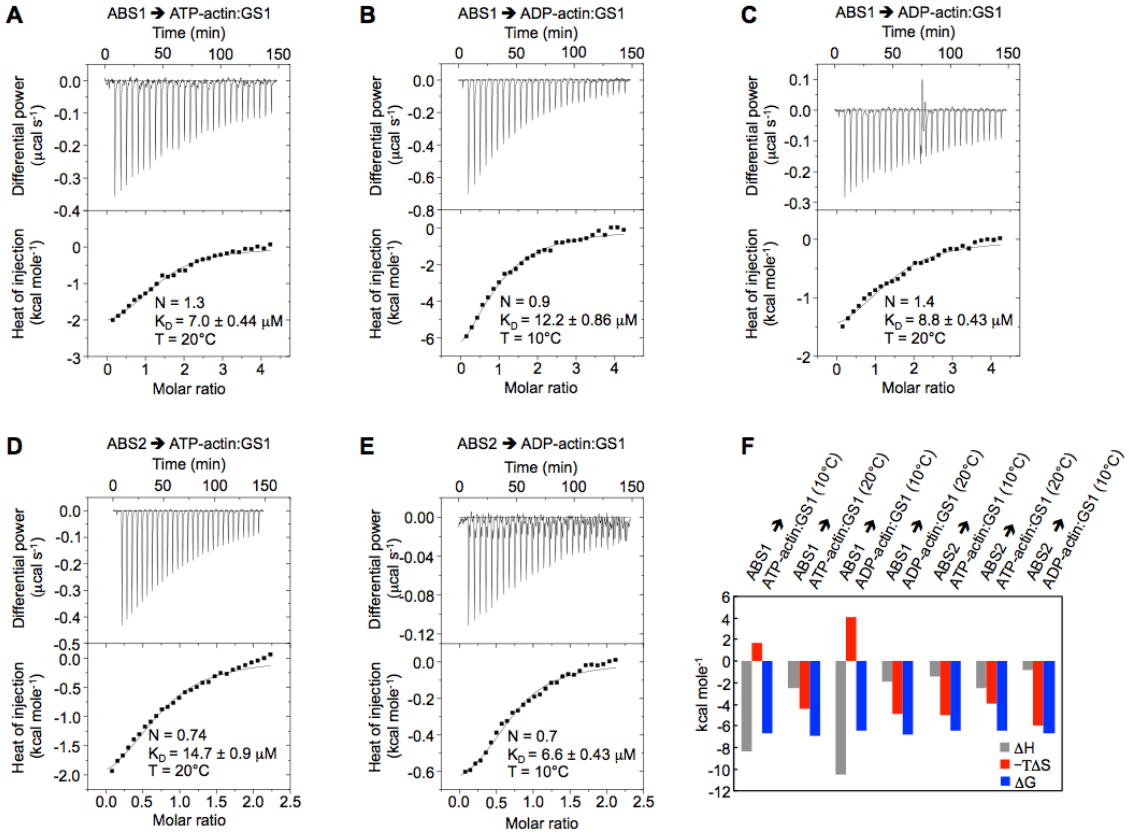

G

Ligand (syringe)	Protein (cell)	10°C K_D (µM)	10°C ΔH (kcal mol^{-1})	10°C ΔS (cal mol^{-1} K^{-1})	20°C K_D (µM)	20°C ΔH (kcal mol^{-1})	20°C ΔS (cal mol^{-1} K^{-1})	ΔC_p (kcal mol^{-1} K^{-1})
ABS1	ATP-actin:GS1	7.5 ± 0.47	-8.38 ± 0.68	-5.81	7.0 ± 0.44	-2.52 ± 0.14	15.0	0.58
ABS1	ADP-actin:GS1	12.2 ± 0.86	-10.46 ± 1.09	-14.3	8.8 ± 0.43	-1.88 ± 0.15	16.7	0.85
ABS2	ATP-actin:GS1	10.5 ± 0.83	-1.43 ± 0.06	17.7	14.7 ± 0.9	-2.53 ± 0.17	13.5	-0.10
ABS2	ADP-actin:GS1	6.6 ± 0.43	-0.77 ± 0.04	21.0				

Fig. S1. Binding of ABS1 and ABS2 to monomeric actin measured by ITC. (**A-E**) ITC titrations of ABS1 and ABS2 into actin:GS1, carried out at different temperatures and with either ATP- or ADP-bound actin:GS1 (as indicated). Conditions are: (**A**-**C**) ABS1 400 µM, actin 20 µM; (**D**) ABS2 632 µM, actin 60 µM; (**E**) ABS2 400 µM, actin 40 µM. (**F**) Schematic representation of the thermodynamic parameters resulting from fitting of the titrations shown in parts **A**-**E**. (**G**) Thermodynamic parameters of the titrations shown in parts **A**-**E**. The reported errors correspond to the s.d. of the fits.

Fig. S2

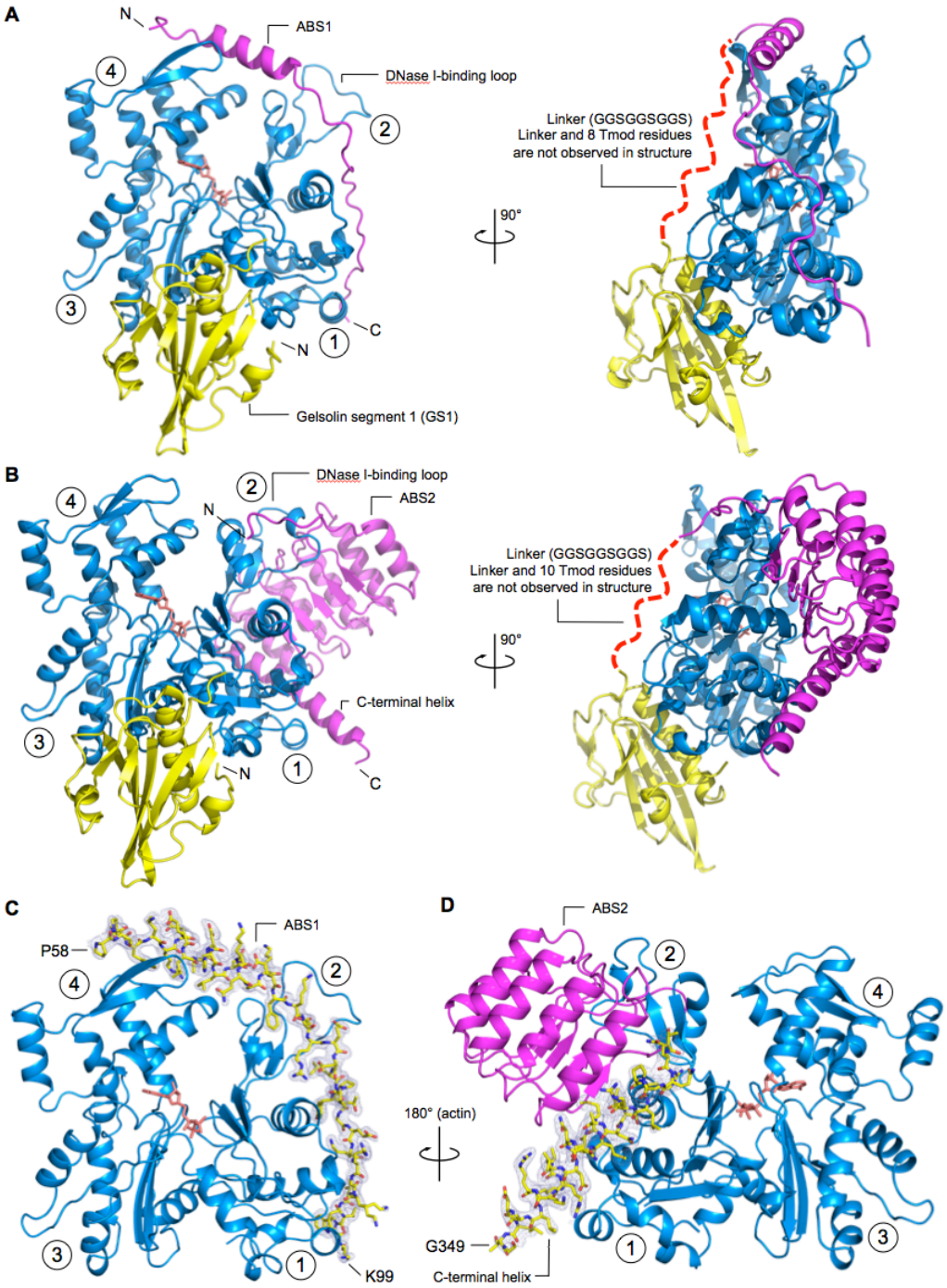

Fig. S2. Structures of Tmod ABS1 and ABS2 bound to actin. (**A**-**B**) Two perpendicular views of the structures of ABS1 and ABS2 (magenta) bound to actin (blue). GS1, which was fused N-terminally to the Tmod fragments via a flexible linker, is shown in yellow. The flexible linkers, which were not observed in the structures, are represented by a discontinuous red line. Circled numbers indicate actin subdomains 1 to 4. (**C**-**D**) Electron density map ($2F_o$-F_c, contoured at 1 σ) around ABS1 and the C-terminal helix of ABS2.

Fig. S3

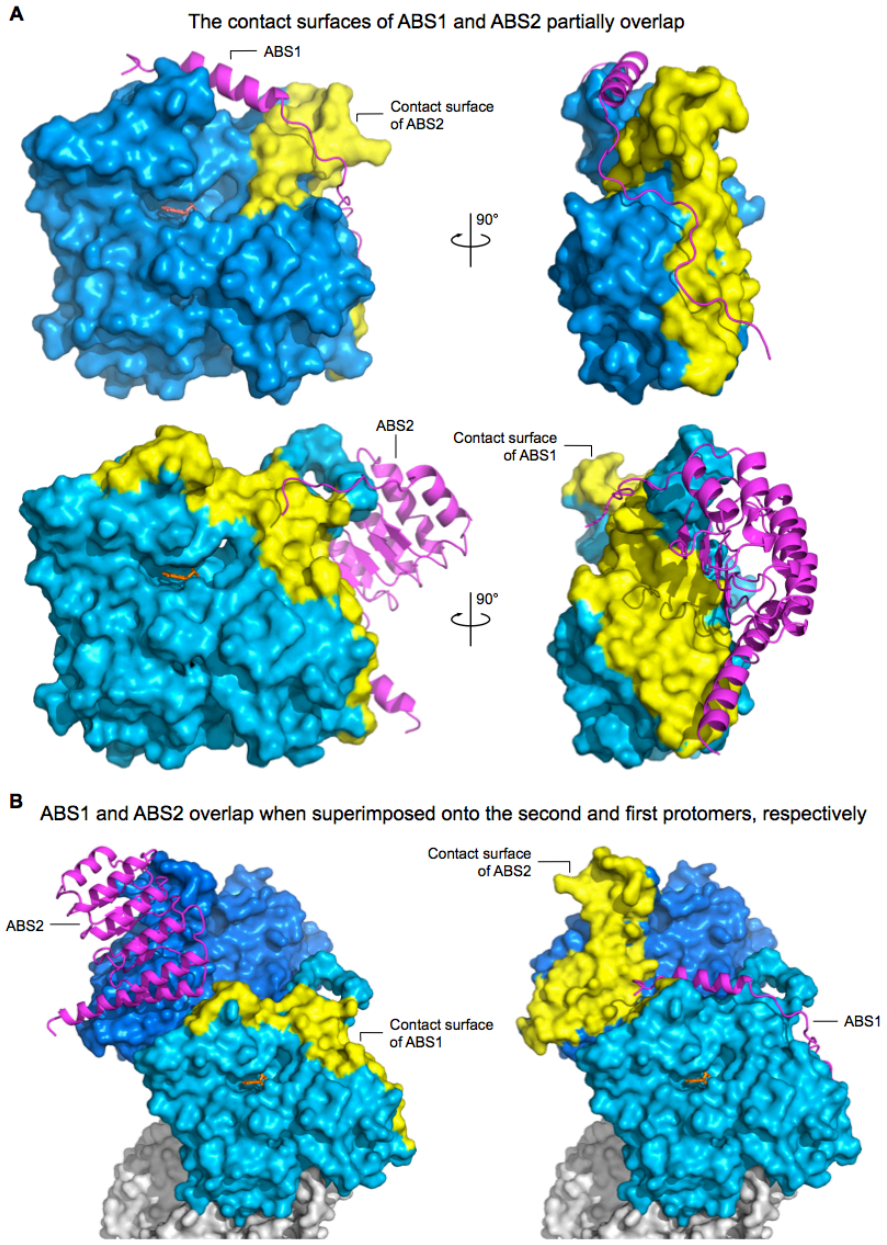

Fig. S3. Determining the location of ABS1 and ABS2 at the pointed end. (**A**) A superimposition of ABS1 (or ABS2) onto the actin portion of the structure of ABS2 (or ABS1) reveals overlap of the contact surfaces (yellow) of the two Tmod domains on actin. (**B**) The binding surfaces of ABS1 and ABS2 also overlap if they are superimposed onto the second and first protomers of the filament, respectively. Therefore, ABS1 and ABS2 must interact with two different protomers at the pointed end, with ABS1 and ABS2 binding to the first and second protomers of the filament, respectively (as shown in Fig. 2A).

Fig. S4

Interactions of Tmod with TM and actin and location of published and current mutations on a sequence alignment of Tmod isoforms and a domain diagram of human Tmod1. Residues interacting with actin protomers 1, 2 and 3 of the filament tend to be highly conserved.

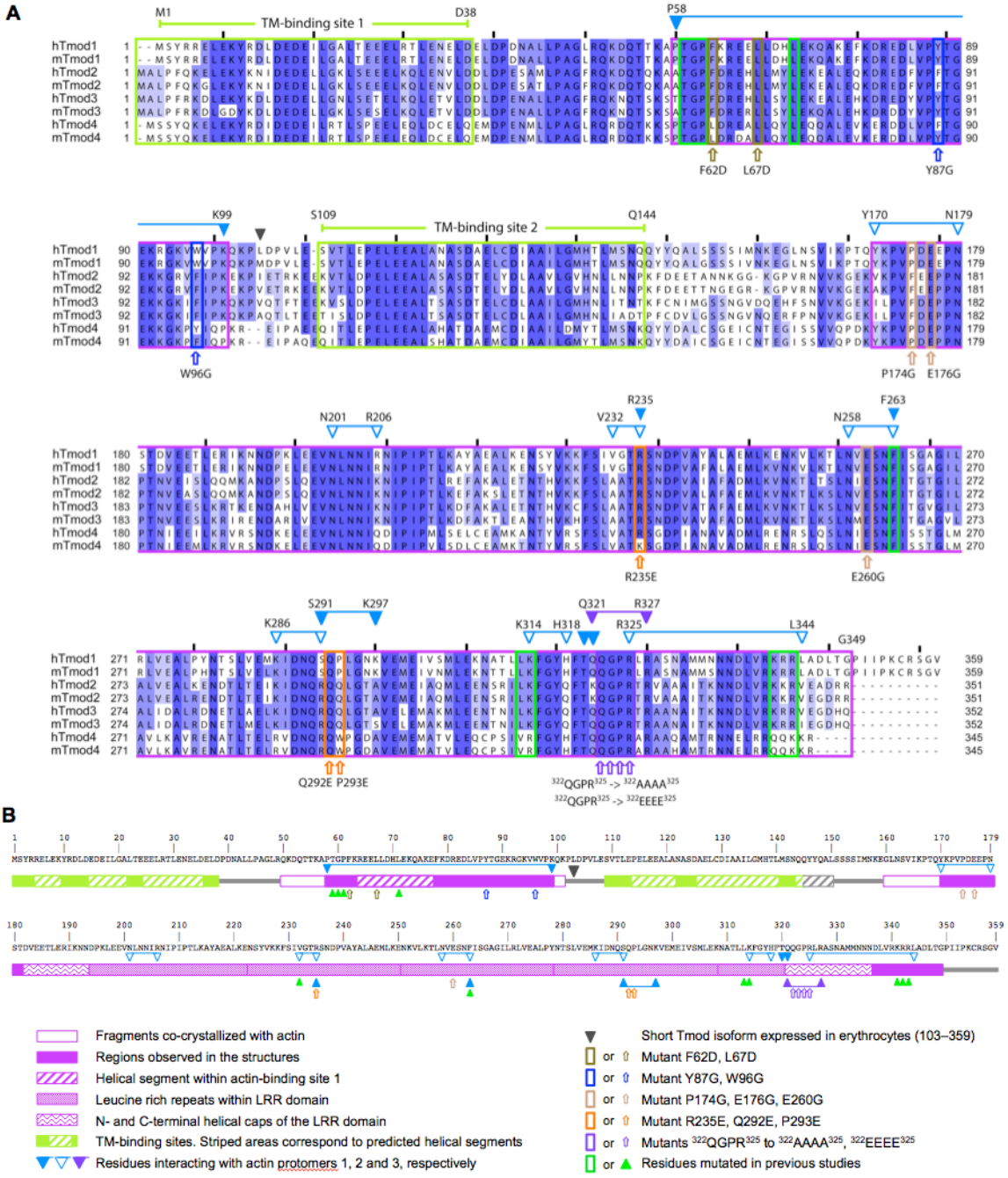

Fig. S4. Mapping of Tmod mutations. (**A**) Representation of the mutants studied here on a sequence alignment of human (h) and mouse (m) Tmod isoforms. Also shows are previously performed mutations and the interactions of Tmod with the first three protomers at the pointed end (keys given on the bottom). (**B**) Domain diagram depicting the mutants and interactions shown in part A (according to Fig. 1A in main text). For reference, the sequence of human Tmod1 is listed along the domain diagram.

Fig. S5

The location of ABS1 and ABS2 is consistent with the two extreme positions of TM on both sides of the actin filament, blocked and open. The linkages between the actin- and TM-binding sites of Tmod must be flexible enough to allow for this movement of TM

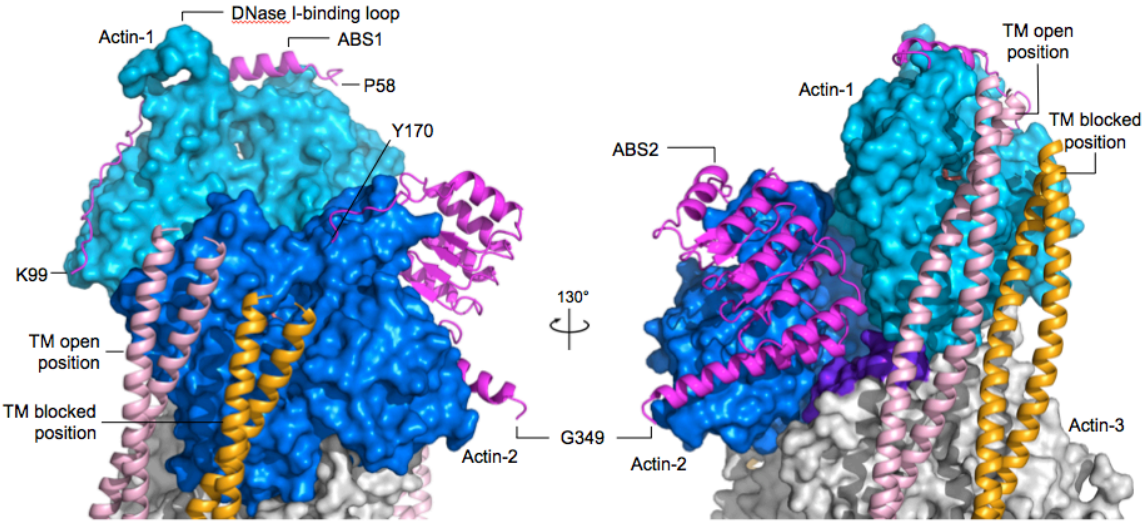

Fig. S5. The binding site of Tmod is sterically compatible with the sliding of TM on the filament. The TM coiled coil binds symmetrically on both sides of the actin filament, forming a continuous rope through overlapping interactions of the C-terminus of each molecule with the N-terminus of the following one (*56*). Like the actin filament, the TM polymer has a defined polarity, with its N- and C-termini directed toward the pointed and barbed ends of the actin filament, respectively. The TM coiled coil has internal pseudo-symmetry, and in muscle sarcomers it consists of 7 pseudo-repeats, each ~40-aa long, that interact with seven actin subunits along the long pitch helix of the actin filament. TM adopts three major positions on the actin filament: blocked, closed, and open (*22, 54*). When bound alone, or in complex with Ca^{+2}-free troponin, TM adopts the most stable blocked position, which masks the binding sites of myosin on the actin filament. The binding of Ca^{2+} to troponin induces a ~25° azimuthal sliding of TM to the intermediate closed position, where the myosin binding sites are partially exposed. Myosin binding to the filament induces an additional ~10° azimuthal sliding of TM to the open position. The blocked position of TM on the filament has been determined using a combination of EM reconstruction and consolidation of crystal structures of TM fragments into a single polypeptide by molecular dynamics (*23*). Another study (*24*), reported an 8 Å-resolution structure of the actin-TM-myosin complex determined by cryo-EM, which defines the open conformation of TM on the filament. Combined, these studies provide the most accurate description available of the two extreme positions of TM on the filament. The sliding of TM on both sides of the filament substantially restricts the available surface for Tmod binding at the pointed end. Yet, Tmod ABS1 and ABS2 are sterically compatible with the two extreme positions of TM. What is more, the proximity of the N-termini of the two Tmod domains to the N-termini of TM is consistent with the expected location of the two TM-binding sites of Tmod. The sequences connecting the two TM-binding sites to the two actin-binding sites of Tmod (E39-A57 and S151-Q169) must be flexible enough to allow for the unobstructed movement of TM (see also Fig. 3 and movie S4).

Fig. S6

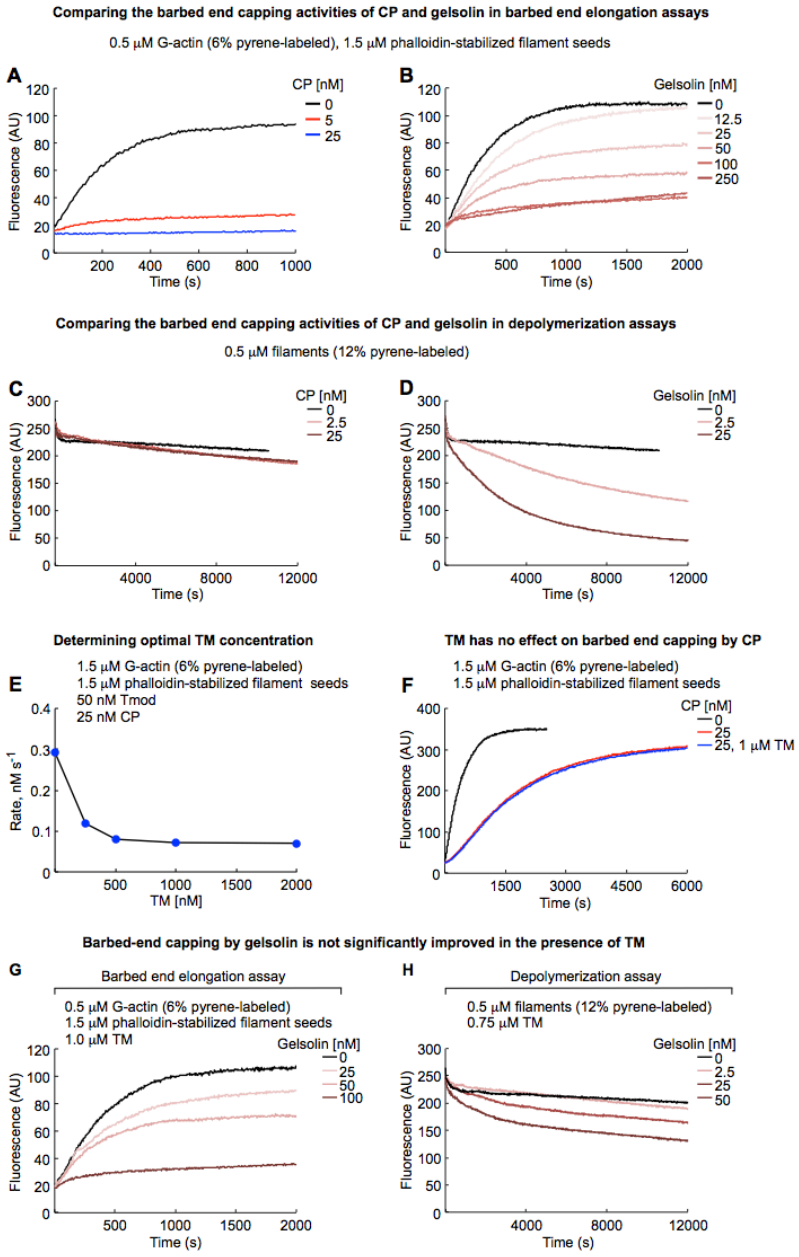

Fig. S6. Finding optimal conditions for pointed end capping experiments. (**A**-**B**) Time course of barbed end elongation of phalloidin-stabilized filament seeds as a function of CP or gelsolin concentration (conditions given on top). (**C**-**D**) Time course of depolymerization of actin filaments as a function of CP or gelsolin concentration. (**E**) Pointed end elongation rate of filament seeds as a function of TM concentration in the presence of 50 nM Tmod. (**F**) Inhibition of barbed end elongation of phalloidin-stabilized filament seeds in the presence of CP or CP and TM. (**G**) Time course of barbed end elongation of phalloidin-stabilized filament seeds as a function of gelsolin concentration in the presence of TM. (**H**) Time course of depolymerization of actin filaments as a function of gelsolin concentration in the presence of TM.

Fig. S7

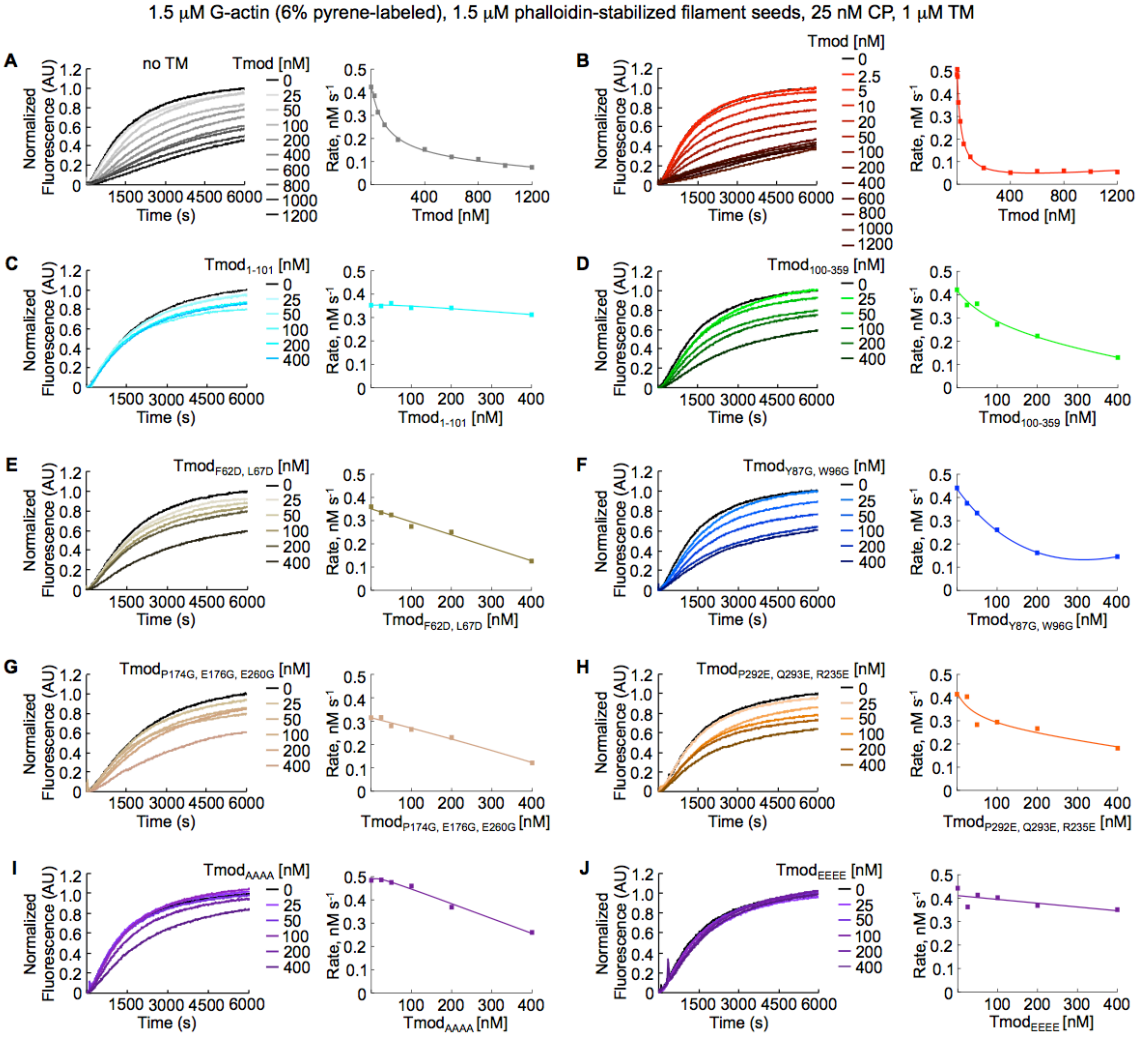

Fig. S7. Pointed end elongation with Tmod and Tmod mutants. (**A**-**J**) Time course of pointed end elongation of phalloidin-stabilized filament seeds as a function of wild type or mutant Tmod concentration, and in the presence of TM (conditions given on top). Polymerization rates (shown on the right of each panel) were calculated for each curve as the slope of the polymerization between 0.1 and 0.4 of the maximum fluorescence normalized to the actin control, and converted to nM s^{-1} (nM monomers adding to filaments s^{-1}), assuming a total concentration of polymerizable actin of 0.9 μM (see materials and methods).

Fig. S8

The interaction of Tmod's ABS2 at the interface of the first three subunits of the actin filament is reminiscent of the interaction of *Vibrio* VopL's VCD at the pointed end. VopL has a repeat of three WH2 domains that make it a strong nucleator. The Tmod-related protein Lmod, which has a WH2 as part of a C-terminal extension, is also an actin nucleator

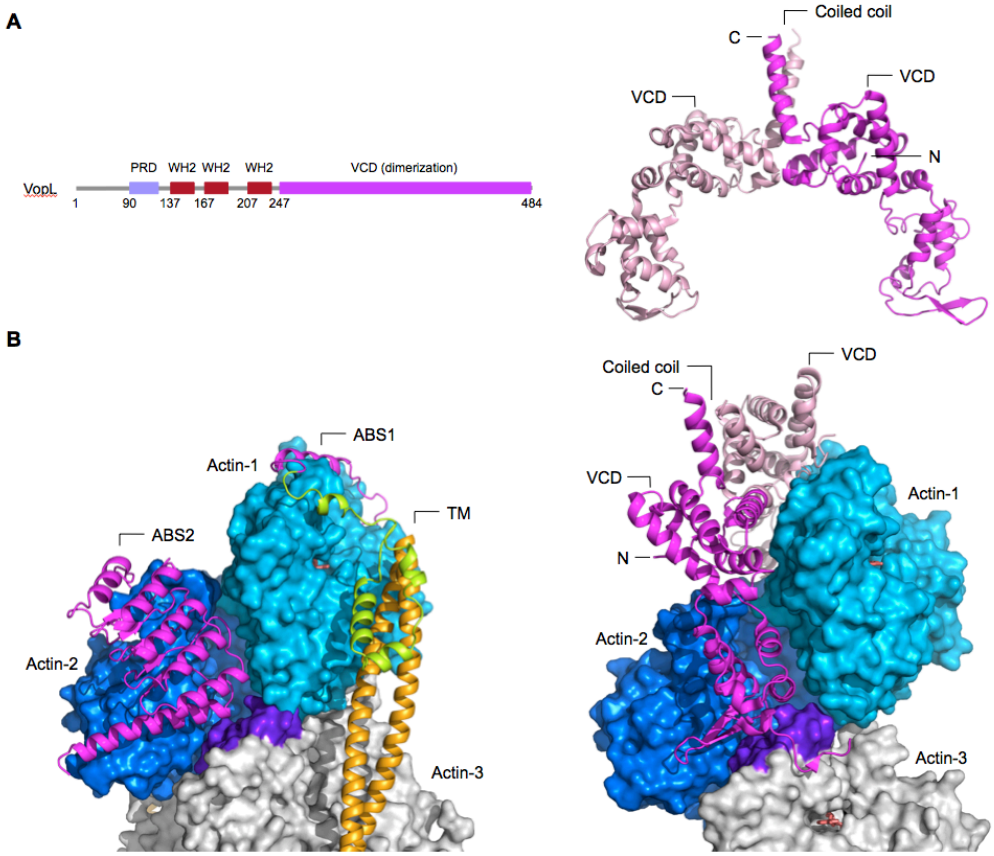

Fig. S8. Similarity of the interactions of Tmod and *Vibrio* VopL at the pointed end. (**A**) Some *Vibrio* species, including *V. parahaemolyticus* and *V. cholera*, produce a type III secretion system (T3SS) virulence factor that has strong actin nucleation activity. Here we show VopL, the protein secreted by the bacterium *V. parahaemolyticus*. VopL has a repeat of three WH2 domains and a *Vibrio* C-terminal domain (VCD). The VCD is responsible for VopL dimerization, which duplicates the number of WH2 domains, and it also mediates binding to the pointed end of the actin filament (*27, 28*). Optimal nucleation activity requires all three of the WH2 domains as well as the VCD, whose structure was first determined in isolation (*27, 28*). (**B**) Recently, the structure of VCD was also determined in complex with an actin trimer (*26*). In the structure, the actin subunits adopt a filament-like arrangement, and one of the arms of the VCD dimer binds at the interface between the three subunits of the actin trimer. The interaction strongly resembles that of the ABS2 of Tmod (shown side-by-side for comparison), despite their different folds. Remarkably, the Tmod-related protein leiomodin (Lmod) is a filament nucleator, like VopL. The main difference between Lmod and Tmod is the presence of a C-terminal extension in Lmod, featuring a WH2 domain. In this way, two unrelated proteins, a bacterial and a eukaryotic protein, share similar interactions at the pointed end, as well as the ability to nucleate actin polymerization when combined with WH2 domain-containing sequences.

Movie S1. Structure of ABS1 bound to actin. 360° rotation of the structure of Tmod ABS1 (magenta) bound to ATP-actin (blue). The side chains of ABS1 are colored by atom type (carbon, yellow; oxygen, red; nitrogen, blue). Movie related to figure 1D in main text.

Movie S2. Structure of ABS2 bound to actin. 360° rotation of the structure of Tmod ABS2 (magenta) bound to ATP-actin (blue). The side chains of ABS2 that fall near actin are also shown, and colored by atom type (carbon, yellow; oxygen, red; nitrogen, blue). Movie related to figure 1E in main text.

Movie S3. Testing the interactions of Tmod at the pointed end by mutagenesis. 360° rotation of the pointed end of the actin filament, with the structures of ABS1 and ABS2 superimposed onto the first and second protomers of the filament, respectively. The side chains of previously mutated residues (*9, 16-18*) (green) and residues mutated here (colored by atom type: carbon, yellow; oxygen, red; nitrogen, blue) are shown. Movie related to figure 2A in main text.

Movie S4. Model of the pointed end. Movie showing a model of the pointed end of the actin filament (*21*), with the structures of the complexes of actin (blue) with ABS1 and ABS2 (magenta) superimposed onto the first and second protomers of the filament, respectively. TM is shown in the stable 'blocked' position, which it assumes when bound to the filament alone or in complex with Ca^{2+}-free troponin (*23*). A tentative model of the two TM-binding sites of Tmod (green) is also shown for reference (see materials and methods for details about modeling of the TM-binding sites). Movie related to figure 3 in main text.

Table S1. Crystallographic Data and Refinement Statistics.

	GS1-ABS1:ATP-actin	GS1-ABS1:ADP-actin [b]	GS1-ABS2:ATP-actin
Data collection			
Space group	P 2_1 2_1 2_1	P 2_1	P 2_1 2_1 2_1
Cell dimensions			
a, *b*, *c* (Å)	69.47, 75.87, 136.40	69.22, 135.14, 40.55	69.39, 81.21, 170.71
α, β, γ (°)	90.0, 90.0, 90.0	90.0, 94.41, 90.0	90.0, 90.0, 90.0
Wavelength (Å)	1.0	1.0781	1.0781
Resolution (Å)	40.0-1.80 (1.91-1.80) [a]	46.0-2.15 (2.28-2.15)	45.0-2.3 (2.44-2.30)
R_{merge} (%)	5.0 (57.6)	7.7 (46.3)	6.3 (57.5)
I / σ I	43.7 (2.5)	17.0 (2.0)	32.8 (3.1)
No. unique reflections	67523	138151	43742
Completeness (%)	99.8 (99.4)	98.7 (99.4)	99.9 (100.0)
Redundancy	13.4 (8.2)	5.9 (5.6)	12.8 (12.2)
Wilson B-factor (Å^2)	27.2	34.8	40.5
Refinement			
Resolution (Å)	40.0-1.8 (1.86-1.80)	44.9-2.15 (2.22-2.15)	45.0-2.3 (2.38-2.30)
No. reflections	67450 (6559)	138122 (13549)	43679 (4227)
R_{work} (%)	15.62 (26.38)	27.42 (33.88)	16.82 (24.32)
R_{free} (%)	18.70 (29.58)	32.62 (38.35)	20.05 (27.22)
No. residues	541	2019	681
No. atoms	4905	16470	5617
Protein	4360	15802	5375
Ligand	34	120	34
Solvent	511	548	208
R.m.s deviations			
Bond lengths (Å)	0.011	0.018	0.014
Bond angles (°)	1.31	1.74	1.43
B-factors (Å^2)	41.5	63.6	53.9
Protein	41.2	64.4	54.3
Ligand	26.7	42.7	39.2
Solvent	45.7	44.2	48.3
Ramachandran (%)			
Favored	99.0	96.0	95.0
Outliers	0.18	0.30	0.59
PDB Code	4PKG	4PKH	4PKI

X-ray datasets were collected at NSLS beamline X6A on:
GS1-ABS1:ATP-actin: Oct 10, 2012
GS1-ABS2:ATP-actin: Jan 22, 2013
GS1-ABS1:ADP-actin: Mar 6, 2013

[a] Values in parenthesis correspond to highest resolution shell

[b] Note that the GS1-ABS1:ADP-actin structure contained four complexes in the asymmetric unit, two of which were poorly ordered, explaining the relatively poor refinement statistics.

Supplementary References:

30. J. D. Pardee, J. A. Spudich, Purification of muscle actin. *Methods Enzymol.* **85 Pt B**, 164 (1982).
31. L. B. Smillie, Preparation and identification of alpha- and beta-tropomyosins. *Methods Enzymol.* **85 Pt B**, 234 (1982).
32. W. Kabsch, H. G. Mannherz, D. Suck, E. F. Pai, K. C. Holmes, Atomic structure of the actin:DNase I complex. *Nature* **347**, 37 (1990).
33. C. E. Schutt, J. C. Myslik, M. D. Rozycki, N. C. Goonesekere, U. Lindberg, The structure of crystalline profilin-beta-actin. *Nature* **365**, 810 (1993).
34. P. J. McLaughlin, J. T. Gooch, H. G. Mannherz, A. G. Weeds, Structure of gelsolin segment 1-actin complex and the mechanism of filament severing. *Nature* **364**, 685 (1993).
35. L. R. Otterbein, C. Cosio, P. Graceffa, R. Dominguez, Crystal structures of the vitamin D-binding protein and its complex with actin: structural basis of the actin-scavenger system. *Proc. Natl. Acad. Sci. U.S.A.* **99**, 8003 (2002).
36. S. H. Lee, D. B. Hayes, G. Rebowski, I. Tardieux, R. Dominguez, Toxofilin from Toxoplasma gondii forms a ternary complex with an antiparallel actin dimer. *Proc. Natl. Acad. Sci. U.S.A.* **104**, 16122 (Oct 9, 2007).
37. V. O. Paavilainen, E. Oksanen, A. Goldman, P. Lappalainen, Structure of the actin-depolymerizing factor homology domain in complex with actin. *J. Cell. Biol.* **182**, 51 (Jul 14, 2008).
38. W. M. Morton, K. R. Ayscough, P. J. McLaughlin, Latrunculin alters the actin-monomer subunit interface to prevent polymerization. *Nat. Cell. Biol.* **2**, 376 (Jun, 2000).
39. J. S. Allingham, A. Zampella, M. V. D'Auria, I. Rayment, Structures of microfilament destabilizing toxins bound to actin provide insight into toxin design and activity. *Proc. Natl. Acad. Sci. U.S.A.* **102**, 14527 (Oct 11, 2005).
40. L. R. Otterbein, P. Graceffa, R. Dominguez, The crystal structure of uncomplexed actin in the ADP state. *Science* **293**, 708 (Jul 27, 2001).
41. T. Otomo *et al.*, Structural basis of actin filament nucleation and processive capping by a formin homology 2 domain. *Nature* **433**, 488 (Feb 3, 2005).
42. M. A. Rould, Q. Wan, P. B. Joel, S. Lowey, K. M. Trybus, Crystal structures of expressed non-polymerizable monomeric actin in the ADP and ATP states. *J. Biol. Chem.* **281**, 31909 (Oct 20, 2006).
43. F. Ferron, G. Rebowski, S. H. Lee, R. Dominguez, Structural basis for the recruitment of profilin-actin complexes during filament elongation by Ena/VASP. *EMBO J.* **26**, 4597 (Oct 31, 2007).
44. E. Irobi *et al.*, Structural basis of actin sequestration by thymosin-beta4: implications for WH2 proteins. *EMBO J.* **23**, 3599 (Sep 15, 2004).
45. P. D. Adams *et al.*, The Phenix software for automated determination of macromolecular structures. *Methods* **55**, 94 (Sep, 2011).
46. P. Emsley, B. Lohkamp, W. G. Scott, K. Cowtan, Features and development of Coot. *Acta Crystallogr. D Biol. Crystallogr.* **66**, 486 (Apr, 2010).
47. A. S. Kostyukova, S. E. Hitchcock-DeGregori, Effect of the structure of the N terminus of tropomyosin on tropomodulin function. *J. Biol. Chem.* **279**, 5066 (Feb 13, 2004).

48. A. S. Kostyukova, S. E. Hitchcock-Degregori, N. J. Greenfield, Molecular basis of tropomyosin binding to tropomodulin, an actin-capping protein. *J. Mol. Biol.* **372**, 608 (Sep 21, 2007).
49. C. C. Gregorio, A. Weber, M. Bondad, C. R. Pennise, V. M. Fowler, Requirement of pointed-end capping by tropomodulin to maintain actin filament length in embryonic chick cardiac myocytes. *Nature* **377**, 83 (Sep 7, 1995).
50. E. S. Harris, H. N. Higgs, Biochemical analysis of mammalian formin effects on actin dynamics. *Methods Enzymol.* **406**, 190 (2006).
51. R. Ishikawa, S. Yamashiro, F. Matsumura, Differential modulation of actin-severing activity of gelsolin by multiple isoforms of cultured rat cell tropomyosin. Potentiation of protective ability of tropomyosins by 83-kDa nonmuscle caldesmon. *J. Biol. Chem.* **264**, 7490 (May 5, 1989).
52. T. Oda, M. Iwasa, T. Aihara, Y. Maeda, A. Narita, The nature of the globular- to fibrous-actin transition. *Nature* **457**, 441 (Jan 22, 2009).
53. A. Narita, T. Oda, Y. Maeda, Structural basis for the slow dynamics of the actin filament pointed end. *EMBO J.* **30**, 1230 (Apr 6, 2011).
54. D. F. McKillop, M. A. Geeves, Regulation of the interaction between actin and myosin subfragment 1: evidence for three states of the thin filament. *Biophys. J.* **65**, 693 (Aug, 1993).
55. E. Krissinel, K. Henrick, Inference of macromolecular assemblies from crystalline state. *J. Mol. Biol.* **372**, 774 (Sep 21, 2007).
56. R. Dominguez, Tropomyosin: the gatekeeper's view of the actin filament revealed. *Biophys. J.* **100**, 797 (Feb 16, 2011).